Research in Astronomy and Astrophysics, 25:055006 (11pp), 2025 May

https://doi.org/10.1088/1674-4527/adca8f
CSTR: 32081.14.RAA.adca8f

The Photometric Investigation of Totally Eclipsing Contact Binaries NSVS 9023048 and NSVS 2461789

Wei Tao[1], Bin Zhang[1,2,3], and Zhen Zhong[1]
[1] School of Physics and Electronic Science, Guizhou Normal University, Guiyang 550001, China; zhangbin@gznu.edu.cn
[2] National Astronomical Observatories, Chinese Academy of Sciences, Beijing 100101, China
[3] Guizhou Provincial Key Laboratory of Radio Astronomy and Data Processing, Guizhou Normal University, Guiyang 550025, China
Received 2024 December 6; revised 2025 March 26; accepted 2025 March 27; published 2025 May 9

Abstract

In this paper, new light curve fitting and orbital period change analysis of two contact binaries NSVS 9023048 and NSVS 2461789 are presented. We found that both of them are totally eclipsing contact binaries. Our photometric solutions suggest that NSVS 9023048 is a deep contact binary ($q = 10.14, f = 69.2\%$), however, NSVS 2461789 is a shallow one ($f = 24.4\%$, $q = 3.08$). The asymmetric light curves of NSVS 2461789 and NSVS 9023048 can be explained by the star-spot activity. At the same time, using the available eclipse times, we first studied the orbital period changes of these two targets. It is discovered that the period of NSVS 9023048 is decreasing at a rate of $dP / dt = -1.17 \times 10^{-6}$ day yr^{-1}, which can be explained by mass transfer from the more massive star to the less massive one or angular momentum loss. In addition, the $O - C$ diagrams of NSVS 9023048 and NSVS 2461789 show possible cyclic oscillations with a period of 7.29 yr and 9.91 yr, respectively. The cyclic oscillations may be caused by the light-travel time effect due to the presence of a third component. The mass of the tertiary companion is determined to be $M_3 \sin(i_3) = 9.05\, M_\odot$ for NSVS 9023048 and $M_3 \sin(i_3) = 0.11\, M_\odot$ for NSVS 2461789. Based on our calculations, the third body of NSVS 9023048 may be a black hole candidate. Our study also reveals that NSVS 9023048 is stable now.

Key words: (stars:) binaries: eclipsing – stars: activity – stars: evolution – stars: individual (NSVS 9023048, NSVS 2461789)

1. Introduction

With the development of some sky surveys in the world, such as the All Sky Automated Survey (ASAS; Pojmanski 2002), the Large sky Area Multi-Object Fiber Spectroscopic Telescope (LAMOST; Zhao et al. 2006, 2012), Wide Angle Search for Planets (SuperWASP; Lohr et al. 2015), Catalina Sky Survey (CSS; Sun et al. 2020) and the Transiting Exoplanet Survey Satellite (TESS; Kunimoto et al. 2021), a large number of contact binaries (CBs) have been discovered and reported. CBs are also called W UMa-type binaries with an EW-type light curve (Mateo et al. 1990; Rubenstein & Bailyn 1996; Qian et al. 2018), and many of them were discovered in clusters (Kaluzny 1990; Rucinski 1994; Yan & Mateo 1994; Mazur et al. 1999). The origin of these systems is still an open question (Bradstreet & Guinan 1994; Qian 2003; Stepien 2006), and CBs are good samples to study the merger process, associated physical mechanisms, mass transfer, and the third body in binaries (Eggleton & Kisseleva-Eggleton 2006). Some researchers think that these CBs are formed through the angular momentum loss (AML) of short-period detached binaries (McCarthy et al. 1996; Vilhu 1982; Qian et al. 2017, 2018). When the mass ratio of CBs is less than 0.1, the binary will become a merger candidate (Rasio 1995; Webbink 1976; Stepien 2006; Liu et al. 2023). The formation of blue stragglers and FK Com stars with rapid rotation is believed to be related to binary mergers (Hut 1980; Eggleton & Kiseleva-Eggleton 2001). At present, only one binary merger event has been reported it is red nova V1309 Sco (Mason et al. 2010; Tylenda et al. 2011).

Williams & Roxburgh (1976) suggested that deep CBs have a mass ratio limit. According to Darwin's instability (Rasio 1995; Li & Zhang 2006; Jiang et al. 2010), a CB star will merge when its mass ratio is less than the limit value (Arbutina 2007, 2009; Wadhwa et al. 2021). Hut (1980) proposed that when $\frac{J_{\rm spin}}{J_{\rm orb}}$ is greater than $1/3$, the binary system will undergo a merger event, where $J_{\rm spin}$ and $J_{\rm orb}$ are the spin angular momentum and the orbital angular momentum of the binary star. Rasio (1995) calculated the unstable mass ratio as 0.09 without considering the $J_{\rm spin}$ of the secondary component. Later, in case of $k_1^2 = k_2^2$ (dimensionless rotation radius) and considering the rotation of the secondary component (Li & Zhang 2006), the value of mass ratio limit was calculated as 0.071–0.078. Then, Arbutina (2009) updated that value as $q_{\rm inst} = 0.070$–0.074. Subsequently, Jiang et al. (2010) restricted that value in the range of 0.05–0.105. Using a statistical study with 46 good samples, Yang & Qian (2015) updated this value to 0.044. After that, V1187 Her ($q = 0.044$) was reported (Caton

et al. 2019). A recent study suggested that the unstable mass ratio is related to the contact degree and the mass of the primary component (Wadhwa et al. 2021). At present, TYC 3801-1529-1 is the lowest mass ratio CB with $q = 0.0356$ (Li et al. 2024).

It is found that many of the extremely low mass ratio contact binaries (ELMRCBs) are totally eclipsing contact binaries (TECBs) (Rucinski 2001; Terrell & Wilson 2005; Li et al. 2022). For these TECBs, statistical studies suggested that the mass ratio obtained from the radial velocity (RV) and photometry is almost equal (Pribulla et al. 2003; Li et al. 2021b). In addition, Rucinski (2001) also found that low mass ratio CBs have smaller amplitudes. To understand the physical properties of TECBs, we selected two targets from the Northern Sky Variability Survey database (NSVS; Woźniak et al. 2004).

NSVS 9023048(= [GGM 2006] 9023047) was classified as a CB candidate by the ROTSE-I survey (Gettel et al. 2006). Then, Hoffman et al. (2009) determined its preliminary elements, such as magnitude (Δm) and orbital period (P). In addition, Gaia (Hwang et al. 2020; Mowlavi et al. 2023) and the All Sky Automated Survey for SuperNovae (ASAS-SN, Jayasinghe et al. 2019) also observed this target. NSVS 2461789 (=ASASSN-V J082143.72+634509.8) was also listed as an eclipsing binary star by NSVS (Gettel et al. 2006). After that, Hoffman et al. (2009) reported its orbital period and light curve amplitude. In addition, NSVS 2461789 has also been observed by Gaia and Zwicky Transient Facility (ZTF; Chen et al. 2020). It should be noted that the TESS (Ricker et al. 2014; Ricker et al. 2015) has observations of these two targets. Using the ASAS-SN light curves (LCs), Li et al. (2024) obtained the primitively photometric parameters of NSVS 9023048 and NSVS 2461789.

Section 2 contains the detailed information on the observations and the data reduction. In Section 3, we present the orbital period change analysis of the two targets using the $O - C$ method. In Section 4, we introduce how to fit the photometric LCs and obtain the photometric solutions. The final discussion and conclusions are described in Section 5.

2. Observations

We carried out new photometric LCs of NSVS 2461789 and NSVS 9023048 by using the two telescopes located at the Xinglong Observatory of the National Astronomical Observatories, Chinese Academy of Sciences (NAOC), and the detailed information about these two telescopes is listed as follows: (1) the 60 cm reflector telescope (NAOC-60) has a field of view of $17' \times 17'$, which is equipped with an Andor DU934P-BEX2-DD camera with UBVRI broadband filters (Mu et al. 2024); (2) the 85 cm reflector telescope (NAOC-85) has a primary mirror focal ratio of $F/3$, and the extreme magnitude that can be photographed is 17. In addition, the 85 cm telescope has a high-performance Andor CCD camera with an effective field of view of $32' \times 32'$ (Bai et al. 2018). All of the observed CCD images are reduced using IRAF, including the corrections for the bias and flat. Two stars with similar brightnesses near our target were selected as the comparison star and the check star, and their candidates are listed in Table 1. The observed multiband LCs of NSVS 2461789 and NSVS 9023048 are plotted in Figure 1.

Table 1
Coordinates of the Targets, the Comparison, and the Check Stars

Target	Other Name	α_{2000}	δ_{2000}
Variable star	NSVS 9023048	$23^h19^m48^s.48$	$+36°03'50''.8$
Comparison	TYC 2764-1022-1	$23^h20^m15^s.24$	$+36°08'56''.2$
Check	TYC 2764-1318-1	$23^h19^m15^s.36$	$+36°13'41''.3$
Variable star	NSVS 2461789	$08^h21^m43^s.92$	$+36°45'09''.7$
Comparison	TYC 4129-1960-1	$08^h21^m20^s.16$	$+36°48'05''.1$
Check	TYC 4129-1850-1	$08^h20^m54^s.06$	$+36°46'09''.6$

3. Orbital Period Change Analysis

The orbital period change study of eclipsing binaries is an important way to discuss some issues, such as searching for a third component (Er-gang et al. 2019; Liao et al. 2019), dynamical interactions (Zhou et al. 2016; Li et al. 2018), mass transfer, and AML (Pi et al. 2019). The $O - C$ analysis method is a useful way to study the orbital period variations of close binaries. In this method, O means the light minima times from photometric observation, and C represents the theoretical values calculated by a given ephemeris (Rovithis-Livaniou 2020). Using this method requires many high-precision eclipsing times. So, we searched for all published data from sky surveys in the world, including ASAS-SN, SuperWASP (Pollacco et al. 2006; Butters et al. 2010), ZTF, and TESS. For the TESS data, we note that the light curve of NSVS 2461789 from sector 20 shows a phase-smearing effect, whose exposure time is 30 minutes. It should be noted that we can obtain accurate eclipsing times under the phase-smearing effect by using the method proposed by Li et al. (2020). When we dealt with discontinuous data, such as the data from ASAS-SN and ZTF, we used the method proposed by Li et al. (2020). We shifted the longer time-span data into one period, built a complete phase or half of the phase light curve, and then calculated the minimum data. For the convenience of calculations, we converted all the eclipsing times to BJD.[4]

3.1. NSVS 9023048

Using the Kwee & van Woerden (1956) method, a total of 364 eclipsing times were obtained, which are listed in Table 2. Among them, our observations provided eight eclipsing times,

[4] https://astroutils.astronomy.osu.edu/time/

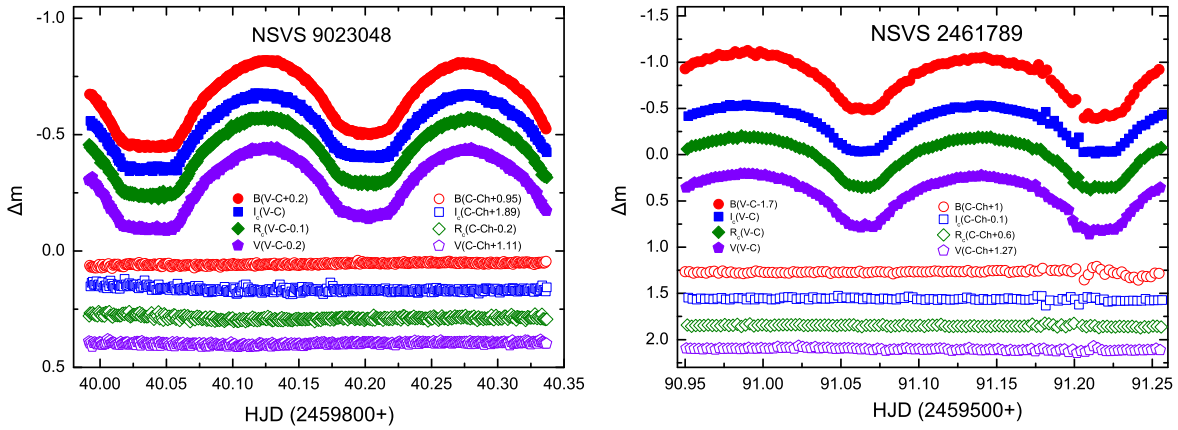

Figure 1. The observed light curves of NSVS 9023048 (left panel) and NSVS 2461789 (right panel) in BVR_cI_c-bands at NAOC.

Table 2
Eclipsing Times of NSVS 9023048

BJD	Error(*day*)	Epoch	$(O-C)(day)$	**Reference**	BJD	Error(*day*)	Epoch	$(O-C)(day)$	**Reference**
2453901.75231	0.00018	0	0.00000	(1)	2459840.03838	0.00065	18266	−0.02706	(3)
2453901.90692	0.00056	0.5	−0.00794	(1)	2459840.20190	0.00039	18266.5	−0.02609	(3)
...	...	...	...	...	...	...	...	...	...
2457503.29146	0.00188	11078	0.05919	(2)	2459855.80821	0.00017	18314.5	−0.02468	(4)
2457592.05216	0.00098	11351	0.06705	(2)	2459855.97157	0.00033	18315	−0.02387	(4)

References: (1) SuperWASP, (2)ASAS-SN, (3) Our observations, (4) TESS.

and others were from the TESS (321), SuperWASP (20), and ASAS-SN (15). Then, its $O-C$ values were calculated using the following linear ephemeris:

$$\text{Min. I(BJD)} = 2453901.75231(\pm 0.00018) + 0^{\text{d}}.325102 \times E. \quad (1)$$

After fitting, we obtained a new ephemeris,

$$\begin{aligned}\text{Min. I(BJD)} = {} & 2453901.78309(\pm 0.00011) \\ & + 0^{\text{d}}.325109839(\pm 0.000000030) \times E \\ & - 5.2005(\pm 0.0136) \times 10^{-10} \times E^2 \\ & + 0.0412267(\pm 0.0001070) \times \sin(0^{\circ}.04397 \\ & \times E + 237^{\circ}.2350^{\circ}(\pm 0^{\circ}.1450))\end{aligned} \quad (2)$$

The $O-C$ diagram of NSVS 9023048 suggests a period decrease superimposed on a possible cyclic oscillation.

3.2. NSVS 2461789

For NSVS 2461789, 11 new eclipsing times were obtained from our observations. In addition, using the data from several sky surveys, we obtained another 328 minima times. Using the following linear ephemeris,

$$\text{Min. I(BJD)} = 2456903.26377(\pm 0.00032) + 0^{\text{d}}.305186 \times E, \quad (3)$$

we calculated the $O-C$ values of NSVS 2461789, which are listed in Table 3. Using the periodic fit, the new ephemeris was derived to be

$$\begin{aligned}\text{Min. I(BJD)} = {} & 2456903.26814(\pm 0.00017) \\ & + 0.\ 305188722(\pm 0.000000021) \times E \\ & + 0.0020873(\pm 0.0007700) \times \sin(0^{\circ}.\ 03037 \\ & \times E - 55^{\circ}.\ 6561(\pm 2^{\circ}.\ 0120)).\end{aligned} \quad (4)$$

The $O-C$ diagram of NSVS 2461789 is also shown in Figure 2 (right panel).

4. Photometric Analysis

Using the 2015 version of the Wilson-Devinney ($W-D$) code (Wilson & Devinney 1971; Wilson 1979; Wilson & Van Hamme 2014), we analyzed the LCs of our two targets. On the basis of the data from the Gaia mission, we obtained the average temperature (primary component) of the two targets. During our analysis, Model 3 (for an over-contact binary) was adopted.

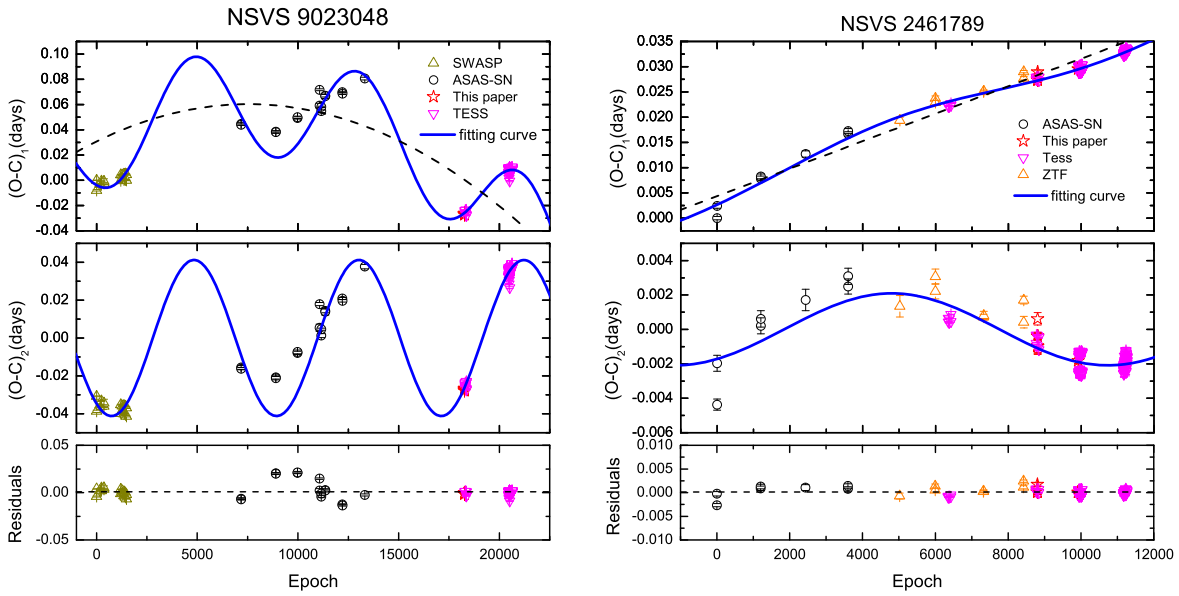

Figure 2. The $O - C$ diagrams of NSVS 9023048 (left panel) and NSVS 2461789 (right panel).

Table 3
Times of Minimum Light for NSVS 2461789

BJD	Error(*day*)	Epoch	$(O - C)(day)$	Reference	BJD	Error(*day*)	Epoch	$(O - C)(day)$	Reference
2456903.26377	0.00032	0	0.00000	(1)	2459591.21683	0.00039	8807.5	0.02736	(2)
2456903.41877	0.00046	0.5	0.00241	(1)	2459591.34882	0.00017	9922	0.02956	(2)
...	...	...	...	...	...	...	...	...	...
2459593.96338	0.00007	8816.5	0.02724	(3)	2460220.97562	0.00035	10871	0.03484	(4)
2459594.11670	0.00006	8817	0.02797	(3)	2460221.12880	0.00057	10871.5	0.03543	(4)

References: (1) ASAS-SN, (2) Our observations, (3) TESS, (4) ZTF.

Adjustable parameters include the effective temperature of the secondary star T_2; the orbital inclination i; the photometric contribution of the primary component L_1; and the dimensionless potentials ($\Omega_1 = \Omega_2$ for over-contact binaries). At the same time, we adopted the limb-darkening coefficients reported by van Hamme (1993). In addition, the coefficients of bolometric albedo and gravity darkening are fixed as $A_1 = A_2 = 0.5$ (Ruciński 1969), and $g_1 = g_2 = 0.32$ (Lucy 1967), respectively.

4.1. NSVS 9023048

Lacking RV curves, a q-search method was used to obtain a possible mass ratio of the target (Li et al. 2019; Terrell 2022). Given that the TESS LC only has one band, we used our multiband LCs to search for a possible mass ratio (q). During our search, we took the q step as 0.1. After multiple attempts, we obtained the results of the q-search with a minimum value of $q = 9.8$, which is plotted in Figure 3. Similar to other TECBs, the q-search curve of NSVS 9023048 shows a sharp bottom (Zhang et al. 2017; Li et al. 2021b). Then, setting q as an adjustable parameter, we continue to fit the LCs with the initial value of q at 9.8. During the fitting process, we found that the TESS LCs from sectors 57 (S57) and 83 (S83) show the negative O'Connell effect (O'Connell 1951). In order to fit these asymmetric TESS LCs, a starspot model was adopted, and we found that a cool starspot on the primary star can get a good convergent solution. Finally, the best photometric solutions are listed in Table 4, and the fitting LCs are plotted in Figure 4.

4.2. NSVS 2461789

Using the same method, we also analyzed the LCs of NSVS 2461789. The results of the q-search are shown in Figure 3 (right panel) with a minimum value at $q = 3.0$. At the same time, we found that NSVS 2461789 was observed several times by the TESS (S20, S47, S60, and S74). It should be noted that the TESS LC from S20 shows a phase-smearing effect, so this set of LC was not adopted in our photometric analysis. In addition, the TESS LCs of S47, S60, and S74 show the O'Connell effect, and

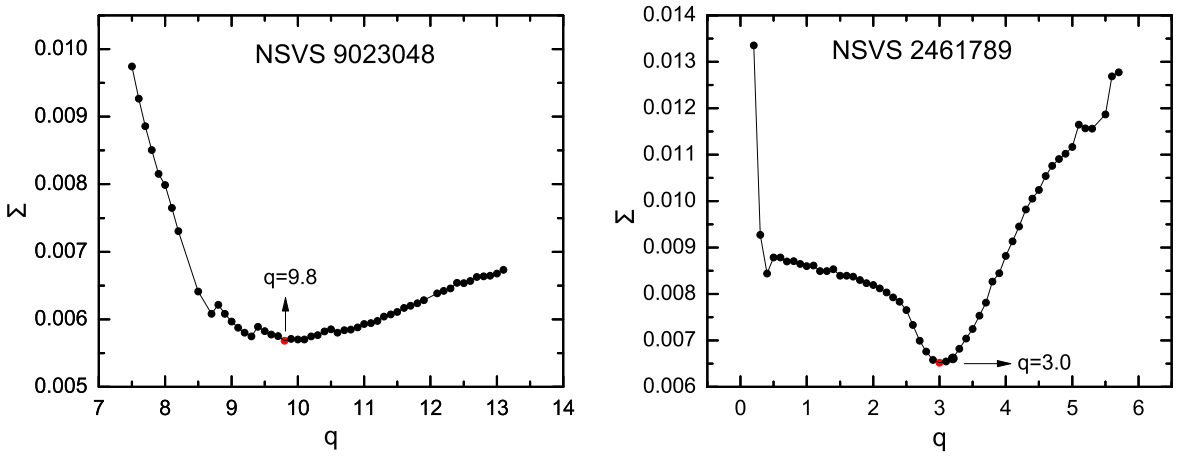

Figure 3. The q-search curves of NSVS 9023048 and NSVS 2461789 using our observed light curves.

Table 4
Photometric Solutions for NSVS 9023048

Parameter	Our LCs in 2022(NAOC-85)	TESS LCs(S57)	TESS LCs(S83)	Li et al. (2024)
$g_1 = g_2$[a]	0.32	0.32	0.32	…
A_1=A_2[a]	0.50	0.50	0.50	…
$T_1(K)$[a]	5958	5958	5958	5958.3
$q = \frac{M_2}{M_1}$	10.137(± 0.011)	9.943(± 0.005)	10.092(± 0.011)	0.88(± 0.206)
T_2 (K)	5933(± 8)	5761(± 3)	5775(± 5)	5839.1
i (°)	80.48(± 0.14)	80.70(± 0.11)	80.49(± 0.13)	57.00(± 1.50)
$\frac{L_1}{L_1+L_2}$(TESS)	…	0.1391(± 0.0050)	0.1390(± 0.0070)	…
$\frac{L_1}{L_1+L_2}(B)$	0.1223(± 0.0199)	…	…	…
$\frac{L_1}{L_1+L_2}(V)$	0.1213(± 0.0129)	…	…	0.4435
$\frac{L_1}{L_1+L_2}(R_c)$	0.1209(± 0.0125)	…	…	…
$\frac{L_1}{L_1+L_2}(I_c)$	0.1206(± 0.0117)	…	…	…
$\Omega_1 = \Omega_2$	14.9162(± 0.0095)	14.7024(± 0.0083)	14.7873(± 0.0106)	…
r_1(pole)	0.2009(± 0.0002)	0.2018(± 0.0002)	0.2040(± 0.0002)	…
r_1(side)	0.2106(± 0.0002)	0.2114(± 0.0002)	0.2142(± 0.0003)	…
r_1(back)	0.2585(± 0.0007)	0.2589(± 0.0006)	0.2684(± 0.0009)	…
r_2(pole)	0.5448(± 0.0003)	0.5435(± 0.0001)	0.5467(± 0.0003)	…
r_2(side)	0.6128(± 0.0005)	0.6107(± 0.0001)	0.6161(± 0.0006)	…
r_2(back)	0.6333(± 0.0006)	0.6313(± 0.0002)	0.6372(± 0.0007)	…
f(%)	69.2(± 1.5)	49.5(± 1.3)	62.7(± 1.6)	29.7(± 6.4)
Spot	Secondary	Primary	Primary	…
Latitude(°)	100.47(± 1.02)	114.74(± 14.84)	144.56(± 1.22)	…
Longitude(°)	180.97(± 0.22)	237.87(± 1.00)	214.69(± 1.00)	…
Radius(°)	14.24[a]	26.85(± 4.81)	45.10 (± 1.04)	…
T_s	0.62(± 0.02)	0.70[a]	0.48[a]	…
Mean residual	0.0045	0.0012	0.0013	…

Note.
[a] Fixed parameters in our analysis.

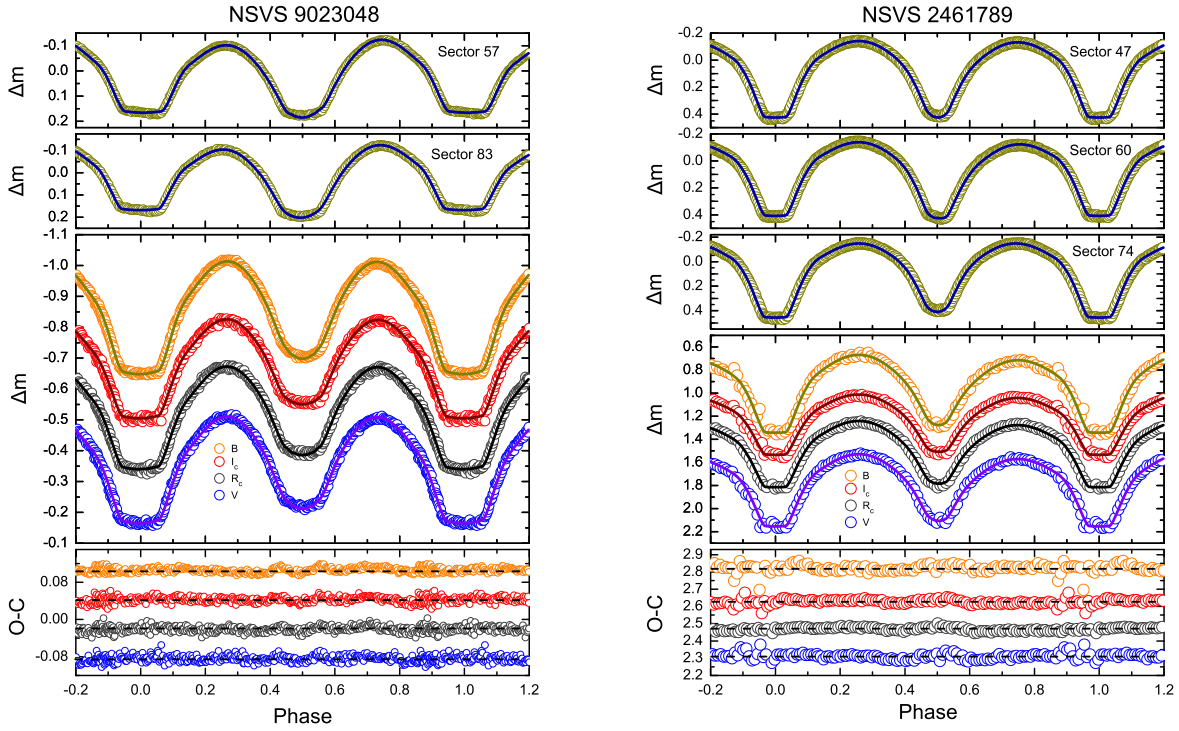

Figure 4. Observed (symbols) and theoretical light curves (solid lines) of NSVS 9023048 and NSVS 2461789 computed from TESS and NAOC.

we also used the starspot model to fit these LCs. The final photometric solutions are listed in Table 5.

5. Discussions and Conclusions

Based on the multicolor LCs of NSVS 9023084 and NSVS 2461789, we obtained their new photometric solutions using the $W-D$ program. The photometric solutions suggest that both of NSVS 9023048 and NSVS 2461789 are W-subtype TECBs. Their asymmetric LCs are caused by the activity of the starspot from the active components. We also studied the orbital period changes of our two targets using the traditional $O-C$ method. It is found that the orbital period of NSVS 9023048 is decreasing at a rate of $dP/dt = -1.17 \times 10^{-6}$ day yr^{-1}, superposed on a possible cyclic oscillation. The $O-C$ diagram of NSVS 2461789 also shows a cyclic variation with an amplitude of 0.0021 day and a period of 9.91 yr.

5.1. Photometric Solutions

Using the data from TESS and our observations, we performed a detailed photometric analysis of NSVS 9023048 and NSVS 2461789. We found that NSVS 9023048 is a deep CB system ($f = 69.2\%$) with a mass ratio of $q = 10.14$. It is discovered that NSVS 2461789 is a shallow W-subtype CB ($f = 24.4\%$) with a small temperature difference ($\Delta T \sim 278K$). In order to explain these asymmetric LCs (showing the O'Connell effect), a cool starspot on the active component is employed (Zhou et al. 2016). Meanwhile, we detected the third light of NSVS 2461789 during our analysis, which is listed in Table 5. Before that, Li et al. (2024) studied these two targets using a machine learning method. Their photometric solutions are also listed in Tables 4 and 5, suggesting that both NSVS 9023048 and NSVS 2461789 are A-subtype CBs. Compared with our photometric solutions, machine learning provides different results. We checked the ASAS-SN LCs for NSVS 9023048 and NSVS 2461789 and found that the data for NSVS 9023048 are somewhat scattered (Poro et al. 2025). For NSVS 2461789, its ASAS-SN LC does not show a clear flat-bottom at phases 0 and 1. So, we believe that the data itself is a possible reason for the different analysis results.

It should be noted that the errors for the parameters listed in Tables 4 and 5 are underestimated, which are only internal uncertainties of the $W-D$ program from the final step of the LC analysis (Xia et al. 2025). As Broens (2013) discussed, in the case of significant nonlinearity, the standard errors are only approximately correct (Liu et al. 2015). In fact, the real uncertainty of these parameters is probably three to five times that of the errors listed in Tables 4 and 5, relying on the required confidence (Popper 1984). Abubekerov et al. (2008, 2009) proposed some correction methods of the error estimates for LC analysis a long time ago. We did not discuss the confidence level of the photometric parameters, so we kept the errors provided by the $W-D$ code.

Table 5
Photometric Solutions for NSVS 2461789

Parameter	Our LCs in 2022(NAOC-60)	TESS LCs(S47)	TESS LCs(S60)	TESS LCs(S74)	Li et al. (2024)
$g_1 = g_2$[a]	0.32	0.32	0.32	0.32	…
$A_1 = A_2$[a]	0.50	0.50	0.50	0.50	…
T_1(K)[a]	5150	5150	5150	5150	5249.0
$q = \frac{M_2}{M_1}$	3.084(± 0.004)	2.984(± 0.002)	2.911(± 0.001)	3.139(± 0.008)	0.27(± 0.02)
T_2(K)	4872(± 15)	4935(± 21)	5025(± 18)	4910(± 19)	5697.5
i(°)	87.60(± 0.40)	88.42(± 0.06)	89.98(± 0.04)	89.52(± 0.17)	80.40(± 1.90)
$\frac{L_1}{L_1+L_2}$(TESS)	…	0.3279(± 0.0057)	0.3060(± 0.0031)	0.3234(± 0.0080)	…
$\frac{L_1}{L_1+L_2}(B)$	0.3595(± 0.0017)	…	…	…	…
$\frac{L_1}{L_1+L_2}(V)$	0.3404(± 0.0022)	…	…	…	0.3253
$\frac{L_1}{L_1+L_2}(R_c)$	0.3262(± 0.0033)	…	…	…	…
$\frac{L_1}{L_1+L_2}(I_c)$	0.3172(± 0.0039)	…	…	…	…
$\frac{L_3}{L_{all}}$(TESS)	…	0.0985(± 0.0016)	0.0692(± 0.0008)	0.0312(± 0.0017)	…
$\frac{L_3}{L_{all}}(B)$	0.0676(± 0.0003)	…	…	…	…
$\frac{L_3}{L_{all}}(V)$	0.0578(± 0.0005)	…	…	…	…
$\frac{L_3}{L_{all}}(R_c)$	0.0746(± 0.0007)	…	…	…	…
$\frac{L_3}{L_{all}}(I_c)$	0.1170(± 0.0009)	…	…	…	…
Ω_1=Ω_2	6.5331(± 0.0026)	6.4818(± 0.0020)	6.4315(± 0.0013)	6.7191(± 0.0097)	…
r_1(pole)	0.2806(± 0.0003)	0.2773(± 0.0001)	0.2758(± 0.0001)	0.2711(± 0.0002)	…
r_1(side)	0.2943(± 0.0004)	0.2900(± 0.0001)	0.2880(± 0.0001)	0.2831(± 0.0003)	…
r_1(back)	0.3389(± 0.0008)	0.3291(± 0.0002)	0.3242(± 0.0002)	0.3201(± 0.0004)	…
r_2(pole)	0.4625(± 0.0002)	0.4546(± 0.0002)	0.4495(± 0.0001)	0.4560(± 0.0008)	…
r_2(side)	0.4997(± 0.0003)	0.4893(± 0.0003)	0.4826(± 0.0002)	0.4907(± 0.0011)	…
r_2(back)	0.5300(± 0.0004)	0.5178(± 0.0003)	0.5101(± 0.0002)	0.5179(± 0.0014)	…
f(%)	24.4(± 0.4)	18.4(± 0.3)	10.7(± 0.2)	12.9(± 1.6)	23.3(± 0.1)
Spot	Secondary	Secondary	Secondary	…	…
Latitude(°)	80.53(± 9.18)	22.91(± 1.57)	99.33(± 0.58)	…	…
Longitude(°)	289.54(± 1.44)	330.40(± 1.01)	335.48(± 0.67)	…	…
Radius(°)	15.04(± 0.23)	21.90[a]	16.67[a]	…	…
T_s	0.82(± 0.01)	0.76(± 0.05)	0.91(± 0.01)	…	…
Mean residual	0.0027	0.0001	0.0012	0.0023	…

Note.
[a] Fixed parameters in our analysis: $L_{all} = L_1 + L_2 + L_3$.

Finally, the empirical formulas provided by Gazeas (2009) were used to estimate the fundamental parameters of our two targets,

$$\log M_1 = 0.725(59) \times \log P - 0.076(32) \times \log q + 0.365(32), \quad (5)$$

$$\log M_2 = 0.725(59) \times \log P + 0.924(33) \times \log q + 0.365(32), \quad (6)$$

$$\log R_1 = 0.930(27) \times \log P - 0.141(14) \times \log q + 0.434(14), \quad (7)$$

$$\log R_2 = 0.930(29) \times \log P + 0.287(15) \times \log q + 0.434(16), \quad (8)$$

$$\log L_1 = 2.531(67) \times \log P - 0.512(51) \times \log q + 1.102(43), \quad (9)$$

$$\log L_2 = 2.531(63) \times \log P + 0.352(52) \times \log q + 1.102(41), \quad (10)$$

where q is mass ratio, P is orbital period, M, R and L are the mass, the radius and the luminosity of the system, respectively. After obtaining the mass of the target, we also calculated the semimajor axis a using Kepler's third law. The calculated parameters are listed in Table 6.

5.2. Orbital Period Variation

The $O - C$ diagram of NSVS 9023048 and NSVS 2461789 exhibits a possible periodic oscillation. In addition, the orbital period of NSVS 9023048 is decreasing at a rate of $dP/dt = -1.17(\pm 0.06) \times 10^{-6}$ day yr^{-1}, which can be explained by AML and/or mass transfer from the more

Table 6
Estimated Parameters for NSVS 9023048 and NSVS 2461789

Parameter	$M_1(M_\odot)$	$M_2(M_\odot)$	$R_1(R_\odot)$	$R_2(R_\odot)$	$L_1(L_\odot)$	$L_2(L_\odot)$	$a(R_\odot)$
NSVS 9023048	0.12	1.22	0.50	1.32	0.33	2.41	2.20
	±0.01	±0.02	±0.02	±0.02	±0.02	±0.01	±0.02
NSVS 2461789	0.35	1.07	0.66	1.06	0.42	1.12	2.14
	±0.02	±0.01	±0.02	±0.01	±0.03	±0.02	±0.03

massive star to the less massive star (Liu et al. 2023). The magnetic activity of the active component (Applegate mechanism) and the light travel time effect (LTTE) due to the presence of a third body are two main explanations of the periodic variation in the $O-C$ diagrams of close binaries (Applegate 1992; Jiang et al. 2010; Hu et al. 2022; Zhang et al. 2025), and they are two completely different physical mechanisms.

If the Applegate mechanism works here, we can test it through calculating the gravitational quadrupole moment ΔQ using the equation (Zhang et al. 2018; Lanza & Rodonò 2002),

$$\triangle P = A\sqrt{2[1-\cos(2\pi P/P_3)]}, \tag{11}$$

$$\frac{\triangle P}{P} = -9\frac{\triangle Q}{M_{1,2}a^2}, \tag{12}$$

where P is orbital period, A is the amplitude of the $O-C$ oscillation, a is the distance between the two components, P_3 is the period of $O-C$ oscillation and M refers to the mass of the active star (Yang et al. 2012). The values of ΔQ for two targets were calculated as follows: (1) for NSVS 9023048, $\Delta Q_1 = 6.04 \times 10^{49}$ g cm^2, $\Delta Q_2 = 6.14 \times 10^{50}$ g cm^2; (2) for NSVS 2461789, $\Delta Q_1 = 6.25 \times 10^{48}$ g cm^2, $\Delta Q_2 = 1.91 \times 10^{49}$ g cm^2. These results are significantly lower than 10^{51}–10^{52} g cm^2, which is a typical value for close binaries under the Applegate mechanism (Lanza & Rodonò 1999; Yang et al. 2014). Based on these results, we think that the Applegate mechanism may not be the main reason for the cycle changes.

Equations (2) and (4) reveal that the $O-C$ oscillation periods for NSVS 9023048 and NSVS 2461789 are 7.29 and 9.91 yr, respectively. Based on the $O-C$ fitting parameters, we calculated the projected radius of the orbit using the following equation:

$$a_{12}\sin i_3 = A_3 \times c, \tag{13}$$

where c and A_3 are the speed of light and the amplitude of the $O-C$ oscillation, respectively, i.e., $a_{12}\sin i_3 = 7.14$ au (NSVS 9023048) and $a_{12}\sin i_3 = 0.36$ au (NSVS 2461789). In addition, we also calculated the mass function,

$$f(m) = \frac{4\pi^2}{GP_3^2} \times (a_{12}\sin i)^3 = \frac{(M_3\sin i)^3}{(M_1+M_2+M_3)^2}. \tag{14}$$

Then the mass of the third body can be calculated as $M_3\sin(i_3) = 9.05\ M_\odot$ (NSVS 9023048) and $M_3\sin(i_3) = 0.11\ M_\odot$ (NSVS 2461789), respectively. The third body of NSVS 2461789 may be a low mass star. The mass of the third body for NSVS 9023048 is large, but we did not detect the third light during our analysis, which means that this third body may be a black hole candidate (Lu et al. 2020; Zhang & Zhang 2024). However, so far, we have not found conclusive evidence showing that this third body is a black hole. All the calculated parameters of the third body are listed in Table 7.

Table 7
$O-C$ Fitting Parameters of NSVS 9023048 and NSVS 2461789

Parameter	P_3 (yr)	A (day)	$a_{12}\sin i$ (au)	$f(m)(M_\odot)$	$M_{3\min}(M_\odot)$
NSVS 9023048	7.29	0.0412	7.14	6.8622	9.05
	±0.64	±0.0001	±0.01	±0.0012	±0.02
NSVS 2461789	9.91	0.0021	0.36	0.0005	0.11
	±0.55	±0.0001	±0.01	±0.0001	±0.01

5.3. Analysis of Orbital Stability

We found that NSVS 9023048 is a deep CB with $\frac{1}{q}$ very close to the mass ratio limit ($q_{\min}$) (Rasio 1995; Wadhwa et al. 2021). Hut (1980) reported that the tidal instability will occur when $J_{\rm spin}/J_{\rm orb} > 1/3$ (Arbutina 2007, 2009). So, $J_{\rm spin}/J_{\rm orb}$ is a very important criterion to test the dynamic stability of the CBs (Li & Zhang 2006). It is reported that the ELMRCB may be eventually merge to produce a bright red nova, such as V1309 Sco (Tylenda et al. 2011; Zhou et al. 2016). In order to discuss the orbital stability of NSVS 9023048, its value of $J_{\rm spin}/J_{\rm orb}$ was calculated using the equation proposed by Yang & Qian (2015),

$$\frac{J_{\rm spin}}{J_{\rm orb}} = \frac{1+q}{q}[(k_1r_1)^2 + (k_2r_2)^2q], \tag{15}$$

where k_1 and k_2 refer to the dimensionless radius of gyration, $r_{1,2}$ is the relative radius. When $k_{12} = k_{22} = 0.06$ (Li & Zhang 2006), we calculated the value of $J_{\rm spin}/J_{\rm orb}$ for NSVS 9023048 as 0.246, which is less than 1/3. From this point of view, NSVS 9023048 is now dynamically stable. According to a theory proposed by Li et al. (2021a), the formation of ELMRCBs may have two different channels. For shallow and medium ELMRCBs, the AML of their progenitors (detached binaries with a short period and an extremely low mass ratio) is

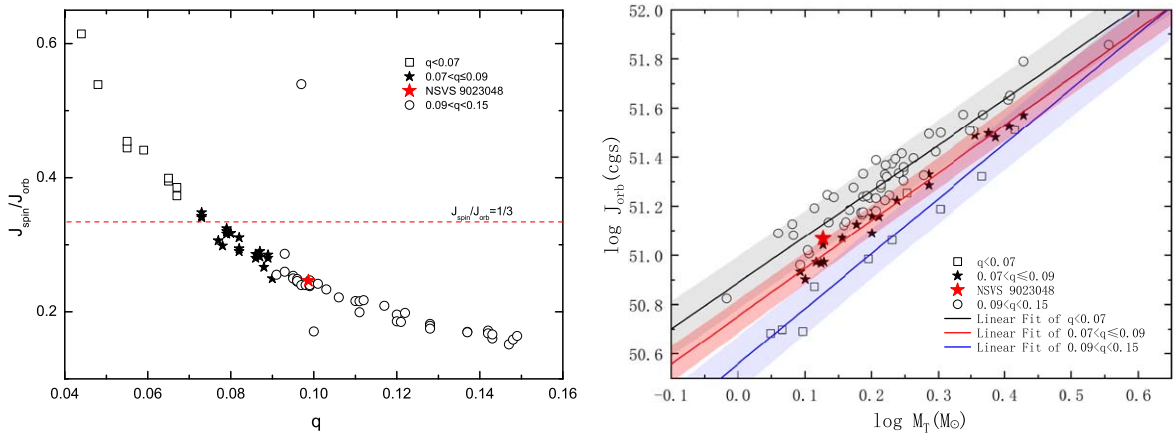

(1) (2)

Figure 5. The relationship of $q - J_{\rm spin}/J_{\rm orb}$ (left panel) and log M_T–log $J_{\rm orb}$ (right panel). In the figure on the left, we adopted $\frac{1}{q} = 0.099$ for NSVS 9023048.

Table 8
Some Contact Binaries with $\frac{J_{\rm spin}}{J_{\rm orb}}$ more than $\frac{1}{3}$

Name	$P(day)$	$q(M_2/M_1)$	$M_1(M_\odot)$	$M_2(M_\odot)$	$R_1(R_\odot)$	$R_2(R_\odot)$	$T_1(K)$	$T_2(K)$	$f(\%)$	$J_{\rm spin}/J_{\rm orb}$	Reference
V1187 Her	0.310760	0.044	1.200	0.050	1.370	0.380	6250	6651	80.00	0.6147	Caton et al. (2019)
TYC 4002-2628-1	0.367058	0.048	1.110	0.054	1.450	0.390	6032	6044	5.00	0.5389	Guo et al. (2022)
VSX J082700.8 +462850	0.277158	0.055	1.060	0.060	1.150	0.320	5870	5828	19.00	0.4446	Li et al. (2021a)
IP Lyn	0.489115	0.055	1.903	0.105	2.070	0.586	6677	6410	21.40	0.4546	Yin et al. (2023)
KIC 4244929	0.341403	0.059	1.481	0.087	1.521	0.477	5857	5867	81.00	0.4411	Şenavcı et al. (2016)
V857 Her	0.382231	0.065	2.180	0.142	1.854	0.616	8300	8513	83.80	0.3949	Qian et al. (2005)
ASAS J083241 +2332.4	0.311300	0.065	1.220	0.080	1.340	0.420	6300	6667	50.65	0.3996	Sriram et al. (2016)
KIC 8539720	0.744499	0.067	2.438	0.163	2.955	0.929	6351	5972	47.00	0.3731	Şenavcı et al. (2016)
CW Lyn	0.812401	0.067	1.680	0.110	2.810	0.960	6532	6284	···	0.3857	Selam (2004); Pribulla et al. (2009)
KIC 3127873	0.671526	0.073	2.268	0.166	2.690	0.899	6069	5791	65.00	0.3427	Şenavcı et al. (2016)
KIC 12352712	0.722065	0.073	2.377	0.174	2.859	0.944	6667	6399	57.00	0.3406	Şenavcı et al. (2016)
ASAS J104422- 0711.2	0.611711	0.073	1.480	0.110	2.210	0.760	7200	7190	83.00	0.3481	Wadhwa et al. (2023)
NSVS 2569022	0.287797	0.077	1.170	0.090	1.190	0.380	6100	6100	1.40	0.3063	Kjurkchieva et al. (2018)
KIC 11097678	0.999716	0.097	0.960	0.189	3.897	1.264	6493	6426	87.00	0.5396	Şenavcı et al. (2016)

the main reason. However, for these deep systems, they may undergo mass transfer from a less massive component to a more massive component. These ELMRCBs are currents at a late stage of their evolution, with mass loss from the outer Lagrangian point. The fill-out factor of NSVS 9023048 will increase along with the orbit decrease in the future.

In addition, we collected some potential unstable systems (Waqas Zubairi et al. 2024) and listed their parameters in Table 8. According to the theories of Rasio (1995) and Arbutina (2007, 2009), we divided these CBs into three parts using $q = 0.07$ and $q = 0.09$ as divisions. Using these data, we analyzed the relationships of $q - J_{\rm spin}/J_{\rm orb}$ and log M − log$J_{\rm orb}$, which are shown in Figure 5. The $J_{\rm orb}$ was estimated using the following formula:

$$J_{\rm orb} = 1.24 \times 10^{52} \times M_T^{5/3} \times P^{1/3} \times q \times (1+q)^{-2}, \quad (16)$$

where M_T is the total mass of the system in solar units, P is the orbital period in days.

In the left panel of Figure 5, we can see that NSVS 9023048 (labeled as a red solid pentagram) is below the instability criterion line ($J_{\rm spin}/J_{\rm orb} = 1/3$). We also noted that some systems located above this red line have not yet merged, which may be caused by the adopted value of gyration radii (k^2) greater than 0.06 (Li et al. 2021b). It can be seen that the value

of k affects the mass ratio limit of CBs. According to a recent study, this limit value can be as low as 0.038 after considering new values of k^2 (Waqas Zubairi et al. 2024). Based on the trend of this diagram, we guess that the ratio of $J_{\rm spin}$ and $J_{\rm orb}$ for ELMRCBs will increase as the mass ratio decreases.

For the data plotted in the right panel of Figure 5, we tried to fit them with different linear formulas. The obtained linear fitting equations are as follows,

$$\log(J_{\rm orb}) = 1.870(\pm0.085) \times \log(M_T) + 50.889(\pm0.021) \quad 0.09 < q < 0.15, \quad (17)$$

$$\log(J_{\rm orb}) = 1.946(\pm0.059) \times \log(M_T) + 50.752(\pm0.015) \quad 0.07 < q \leqslant 0.09, \quad (18)$$

$$\log(J_{\rm orb}) = 2.140(\pm0.145) \times \log(M_T) + 50.596(\pm0.021) \quad q \leqslant 0.07. \quad (19)$$

We note that NSVS 9023048 is near the red solid line. Our fitting formulas reveal that a CB will have a more J_{orb} when its total mass is large. More high-precision observations (photometric and spectroscopic) of ELMRCBs are still needed in the future to verify our results.

Acknowledgments

This work is partly supported by the National Natural Science Foundation of China (Nos. 11988101, U1931101, 42364001 and 11933008), the Foundation of Education Bureau of Guizhou Province, China (No. KY (2020) 003) and the Guizhou Provincial Science and Technology Foundation (No. ZK[2022]322) and the Guizhou Normal University 2019 Special project of training new academics. We acknowledge the support of the staff of the Xinglong 60 and 85 cm telescopes. This work was partially supported by National Astronomical Observatories, Chinese Academy of Sciences. This work includes data collected by the TESS, ASAS-SN, ZTF, and CSS, and we acknowledge the TESS, ASAS-SN, ZTF, and CSS teams for their support. We also appreciate the data from the Gaia mission.

ORCID iDs

Bin Zhang https://orcid.org/0000-0001-7832-2972
Zhen Zhong https://orcid.org/0000-0003-0155-0752

References

Abubekerov, M. K., Gostev, N. Y., & Cherepashchuk, A. M. 2008, ARep, 52, 99
Abubekerov, M. K., Gostev, N. Y., & Cherepashchuk, A. M. 2009, ARep, 53, 722
Applegate, J. H. 1992, ApJ, 385, 621
Arbutina, B. 2007, MNRAS, 377, 1635
Arbutina, B. 2009, MNRAS, 394, 501
Bai, C.-H., Fu, J.-N., Li, T.-R., et al. 2018, RAA, 18, 107
Bradstreet, D. H., & Guinan, E. F. 1994, in ASP Conf. Ser. 56, Interacting Binary Stars, ed. A. W. Shafter (San Francisco, CA: ASP), 228
Broens, E. 2013, MNRAS, 430, 3070
Butters, O. W., West, R. G., Anderson, D. R., et al. 2010, A&A, 520, L10
Caton, D., Gentry, D. R., Samec, R. G., et al. 2019, PASP, 131, 054203
Chen, X., Wang, S., Deng, L., et al. 2020, ApJS, 249, 18
Eggleton, P. P., & Kiseleva-Eggleton, L. 2001, ApJ, 562, 1012
Eggleton, P. P., & Kisseleva-Eggleton, L. 2006, Ap&SS, 304, 75
Er-gang, Z., Sheng-bang, Q., Soonthornthum, B., et al. 2019, ApJL, 871, L10
Gazeas, K. D. 2009, CoAst, 159, 129
Gettel, S. J., Geske, M. T., & McKay, T. A. 2006, AJ, 131, 621
Guo, D.-F., Li, K., Liu, F., et al. 2022, MNRAS, 517, 1928
Hoffman, D. I., Harrison, T. E., & McNamara, B. J. 2009, AJ, 138, 466
Hu, K., Meng, Z.-B., Wang, H.-W., Yu, Y.-X., & Xiang, F.-Y. 2022, PASA, 39, e057
Hut, P. 1980, A&A, 92, 167
Hwang, H.-C., Hamer, J. H., Zakamska, N. L., & Schlaufman, K. C. 2020, MNRAS, 497, 2250
Jayasinghe, T., Stanek, K. Z., Kochanek, C. S., et al. 2019, MNRAS, 486, 1907
Jiang, D., Han, Z., Wang, J., Jiang, T., Li, L., et al. 2010, MNRAS, 405, 2485
Kaluzny, J. 1990, AcA, 40, 61
Kjurkchieva, D. P., Popov, V. A., & Petrov, N. I. 2018, RAA, 18, 129
Kunimoto, M., Huang, C., Tey, E., et al. 2021, RNAAS, 5, 234
Kwee, K. K., & van Woerden, H. 1956, BAN, 12, 327
Wadhwa, S. S., Arbutina, B., Petrović, J., Filipović, M. D., De Horta, A. Y., et al. 2023, PASP, 135, 094201
Lanza, A. F., & Rodonò, M. 1999, A&A, 349, 887
Lanza, A. F., & Rodonò, M. 2002, AN, 323, 424
Li, K., Gao, X., Guo, D.-F., et al. 2024, A&A, 692, L4
Li, K., Gao, X., Liu, X.-Y., et al. 2022, AJ, 164, 202
Li, K., Kim, C.-H., Xia, Q.-Q., et al. 2020, AJ, 159, 189
Li, K., Xia, Q.-Q., Hu, S. M., Guo, D. -F., & Chen, X. 2018, PASP, 130, 074201
Li, K., Xia, Q.-Q., Kim, C.-H., et al. 2021a, ApJ, 922, 122
Li, K., Xia, Q.-Q., Kim, C.-H., et al. 2021b, AJ, 162, 13
Li, K., Xia, Q.-Q., Michel, R., et al. 2019, MNRAS, 485, 4588
Li, L., & Zhang, F. 2006, MNRAS, 369, 2001
Li, X.-Z., Zhu, Q.-F., Ding, X., et al. 2024, ApJS, 271, 32
Liao, W. -P., Qian, S. -B., & Sarotsakulchai, T. 2019, AJ, 157, 207
Liu, N. -P., Qian, S. -B., Soonthornthum, B., et al. 2015, AJ, 149, 148
Liu, X.-Y., Li, K., Michel, R., et al. 2023, MNRAS, 519, 5760
Lohr, M. E., Norton, A. J., Payne, S. G., West, R. G., & Wheatley, P. J. 2015, A&A, 578, A136
Lu, H.-P., Zhang, L.-P., Michel, R., Han, X. -L., et al. 2020, ApJ, 901, 169
Lucy, L. B. 1967, ZA, 65, 89
Mason, E., Diaz, M., Williams, R. E., Preston, G., & Bensby, T. 2010, A&A, 516, A108
Mateo, M., Harris, H. C., Nemec, J., & Olszewski, E. W. 1990, AJ, 100, 469
Mazur, B., Krzeminski, W., & Kaluzny, J. 1999, AcA, 49, 551
McCarthy, P. J., Kapahi, V. K., van Breugel, W., et al. 1996, ApJS, 107, 19
Mowlavi, N., Holl, B., Lecoeur-Taïbi, I., et al. 2023, A&A, 674, A16
Mu, H.-Y., Fan, Z., Zhu, Y.-N., Zhang, Y., & Wu, H. 2024, RAA, 24, 055009
O'Connell, D. J. K. 1951, MNRAS, 111, 642
Pi, Q.-F., Zhang, L.-Y., Bi, S.-L., et al. 2019, ApJ, 877, 75
Pojmanski, G. 2002, AcA, 52, 397
Pollacco, D. L., Skillen, I., Collier Cameron, A., et al. 2006, PASP, 118, 1407
Popper, D. M. 1984, AJ, 89, 132
Poro, A., Li, K., Paki, E., et al. 2025, MNRAS, 537, 3160P
Pribulla, T., Kreiner, J. M., & Tremko, J. 2003, CoSka, 33, 38
Pribulla, T., Rucinski, S. M., Blake, R. M., et al. 2009, AJ, 137, 3655
Qian, S. 2003, MNRAS, 342, 1260
Qian, S.-B., He, J.-J., Zhang, J., et al. 2017, RAA, 17, 087
Qian, S. -B., Zhang, J., He, J. -J., et al. 2018, ApJS, 235, 5
Qian, S. -B., Zhu, L. -Y., Soonthornthum, B., et al. 2005, AJ, 130, 1206
Rasio, F. A. 1995, ApJL, 444, L41
Ricker, G. R., Winn, J. N., Vanderspek, R., et al. 2014, Proc. SPIE, 9143, 914320
Ricker, G. R., Winn, J. N., Vanderspek, R., et al. 2015, JATIS, 1, 014003
Rovithis-Livaniou, H. 2020, Galax, 8, 78
Rubenstein, E. P., & Bailyn, C. D. 1996, AJ, 111, 260
Ruciński, S. M. 1969, AcA, 19, 245
Rucinski, S. M. 1994, JRASC, 88, 252
Rucinski, S. M. 2001, AJ, 122, 1007

Şenavcı, H. V., Doğruel, M. B., Nelson, R. H., Yılmaz, M., & Selam, S. O. 2016, PASA, 33, e043
Selam, S. O. 2004, A&A, 416, 1097
Sriram, K., Malu, S., Choi, C. S., & Vivekananda Rao, P. 2016, AJ, 151, 69
Stepien, K. 2006, AcA, 56, 347
Sun, W., Chen, X., Deng, L., & de Grijs, R. 2020, ApJS, 247, 50
Terrell, D. 2022, Galax, 10, 8
Terrell, D., & Wilson, R. E. 2005, Ap&SS, 296, 221
Tylenda, R., Hajduk, M., Kamiński, T., et al. 2011, A&A, 528, A114
van Hamme, W. 1993, AJ, 106, 2096
Vilhu, O. 1982, A&A, 109, 17
Wadhwa, S. S., De Horta, A., Filipović, M. D., et al. 2021, MNRAS, 501, 229
Waqas Zubairi, A., Ergang, Z., Shengbang, Q., Xiao, Z., & Fernández Lajús, E. 2024, arXiv:2406.05664
Webbink, R. F. 1976, ApJ, 209, 829
Williams, P. S., & Roxburgh, I. W. 1976, MNRAS, 176, 81
Wilson, R. E. 1979, ApJ, 234, 1054
Wilson, R. E., & Devinney, E. J. 1971, ApJ, 166, 605
Wilson, R. E., & Van Hamme, W. 2014, ApJ, 780, 151
Woźniak, P. R., Vestrand, W. T., Akerlof, C. W., et al. 2004, AJ, 127, 2436
Xia, Q., Wang, X., Li, K., et al. 2025, AJ, 169, 139
Yan, L., & Mateo, M. 1994, AJ, 108, 1810
Yang, Y.-G., & Qian, S.-B. 2015, AJ, 150, 69
Yang, Y.-G., Yang, Y., & Li, S.-Z. 2014, AJ, 147, 145
Yang, Y. -G., Zhang, X. -B., Li, H. -L., & Dai, H. -F. 2012, AJ, 144, 136
Yin, Z.-X., Meng, Z.-B., Wu, P.-R., et al. 2023, RAA, 23, 085013
Zhang, B., Gao, Y.-D., Li, K., et al. 2025, MNRAS, 537, 3366
Zhang, B., Qian, S.-B., Michel, R., Soonthornthum, B., & Zhu, L.-Y. 2018, RAA, 18, 030
Zhang, J., Qian, S.-B., Han, Z.-T., & Wu, Y. 2017, MNRAS, 466, 1118
Zhang, X., & Zhang, B. 2024, RAA, 24, 015022
Zhao, G., Chen, Y.-Q., Shi, J.-R., et al. 2006, ChJAA, 6, 265
Zhao, G., Zhao, Y.-H., Chu, Y.-Q., Jing, Y.-P., & Deng, L.-C. 2012, RAA, 12, 723
Zhou, X., Qian, S. -B., Zhang, J., et al. 2016, ApJ, 817, 133